

#### Contents lists available at ScienceDirect

# **Ultrasonics**

journal homepage: www.elsevier.com/locate/ultras



# Check for updates

# Autonomous and ultrasonically assisted drilling in a range of rocks and ice

Xuan Li, Patrick Harkness

Centre for Medical & Industrial Ultrasonics, James Watt School of Engineering, University of Glasgow, UK

ARTICLE INFO

Keywords: UAD Weight-on-bit Torque reduction

#### ABSTRACT

Drilling in extreme environments may require reductions in weight-on-bit, applied torque, or energy use, without compromising rate-of-progress. This paper examines the use of ultrasonic vibration, directly superimposed onto an augering coring bit, to achieve this goal in aircrete, limestone, marble, tuff, and ice.

Compared to traditional rotary drilling processes using the same tool, the ultrasonically assisted drilling processes demonstrated improved rate-of-progress ( $\sim$ 400%) in all materials studied. In aircrete and limestone, there were also modest but consistent reductions in torque power demand and, at optimum vibration amplitudes, total energy consumption ( $\sim$ 25%). The other materials gave more mixed results: ultrasonically assisted drill cycles in marble were energy intensive, those in tuff were unpredictable due to the inconsistencies in that material, and those in ice led to the failure of the tooth bonding.

## 1. Introduction

Drilling in extreme environments can impose limitations on available weight-on-bit, torque, power, and energy. Relevant applications may be found in Antarctic exploration [1], or in space research [2], where terrestrial gravity cannot be relied upon to react the forces and torques required [3,4]. This means that drilling in planetary environments is particularly challenging [5]. To address these issues, the ultrasonic/sonic driller/corer (USDC) technology was developed [6]. This technique uses a Langevin-style ultrasonic transducer to excite a percussive stack that consists of a free mass and a free drilling bit, such that percussive pulses can be transmitted into the rock [7]. The dynamic optimization of the stack is a complex problem [8], and to reach significant depth issues surrounding spoil management still need to be addressed.

Therefore, it would be attractive if more traditional drill tool architectures could operate at reduced weight-on-bit, torque, and energy consumption values. One avenue is based on ultrasonically assisted machining (UAM), which superimposes high frequency ultrasonic vibrations onto a near-traditional tool. This has been shown to reduce weight-on-bit, torque, temperature, and tool wear, across a wide range of difficult-to-cut materials [9-11] in various industrial machining processes. This technique requires stabilization of the vibration response against the nonlinearities that would otherwise be induced by the 'vibro-impact' of the tool against the workpiece [12,13]. Choosing an appropriate feed rate is crucial in UAM, because this maintains some degree of

However, ultrasonically assisted machining (or more accurately ultrasonically assisted drilling, (UAD)) in rocks is quite uncommon, and although some studies have shown its potential in smaller bits of up to 7 mm diameter [14-16], this is the first study to examine the effect when a sizeable drill-bit (21 mm) is managed using an autonomous control loop, as would likely be the case in flight.

This work will include an examination of performance in rocks and ice at a range of targeted weights-on-bit and ultrasonic amplitudes, measuring rate-of-progress, ultrasonic power, torque power, and actuation power, such that any optimum energy settings might be found. The drill cycles will be made horizontally to minimize any separate spoil augering issues, as that is a separate problem.

# 2. Analogue materials for the drilling tests

The materials for the experimental tests are aircrete, limestone, tuff, marble, and ice, as shown in Fig. 1.

Aircrete is a porous construction material made from cement, lime and pulverised fuel ash. Limestone is a sedimentary rock, mostly composed of calcium carbonate ( $CaCO_3$ ) with a homogeneous but slightly granular texture. Marble is metamorphosed limestone, and tuff is lithified volcanic ash. However, unlike the other materials, tuff has random pores, vugs, and inclusions, which makes it behave unpredictably in drilling experiments. The ice is normal water ice,  $I_h$ , made in a

E-mail address: Patrick.Harkness@glasgow.ac.uk (P. Harkness).

tool-workpiece separation and hence allows common stabilization techniques, such as phase-tracking, to be deployed effectively.

<sup>\*</sup> Corresponding author.



Fig. 1. Materials obtained for ultrasonic drilling experiments.

**Table 1**Material properties for drilling experiments.

Material	$\rho$ [kg/m <sup>3</sup> ]	Porosity [%]	Hardness [Mohs]	UCS [MPa]
Aircrete	350	85	_	3.5
Limestone	2550	5.3	3.5	30
Marble	2750	0.49	4	100
Tuff	1955	18.8	3	46
Ice	917	_	1.5	4

freezer from an unboiled mains supply.

The material properties summarised in Table 1 [17-25], where UCS stands for Ultimate Compressive Strength, show that these materials encompass a wide range of material properties. They also cover a wide range of potential substrates in planetary analogue and space environments: aircrete and tuff represent tephra, limestone forms in shallow oceans, and marble is often used as a representative test material for planetary drills. Ice is ubiquitous and challenging throughout.

# 3. Methodology

# 3.1. Ultrasonic drill tool

Fig. 2 presents the custom-designed Ti/6Al/4V ultrasonic drill tool, connected to a Sonic Systems L500 transducer and energised by a Sonic Systems P100 control unit. The tool has a step to boost amplitude, and a two-start auger to extract spoil. Two tungsten carbide teeth are silver-soldered into the cutting face [8], but this is known to be a difficult technique with titanium [26] and tooth failures will be noted as a consequence.

The outer diameter of the coring bit is 21 mm and the central hollow

diameter is 8.5 mm, with a depth of 180 mm. The device operates in the 3rd longitudinal mode (L3), at around 20 kHz, as characterised by an electrical impedance analysis (IA) and an experimental modal analysis (EMA).

#### 3.1.1. Electrical impedance analysis (IA)

The IA measurements were performed using an impedance analyser (4294A, Agilent, Santa Clara), with a swept signal of 1 V peak-to-peak applied. The effective electromechanical coupling coefficient,  $k_{\rm eff}$ , was calculated from the impedance spectrum data using equation (1) [27], providing a measurement of the electromechanical conversion efficiency...

$$k_{\rm eff}^2 = \frac{f_a^2 - f_r^2}{f_a^2} \tag{1}$$

where  $f_a$  is the anti-resonance frequency and  $f_r$  is the resonance frequency.

The mechanical Q factor was also evaluated, as an indicator of the potential to achieve high ultrasonic amplitudes.

# 3.1.2. Experimental modal analysis (EMA)

The EMA was performed by measuring the frequency response functions (FRFs) across a grid of points [28]. A white noise excitation signal was generated by a signal generator (Quattro, Data Physics, San Jose) and amplified by a power amplifier (QSC, RMX 4050HD, Costa Mesa), before being supplied to the transducers. A 3-D laser Doppler vibrometer (CLV3000, Polytec, Waldbronn) was used to measure orthogonal vibration components at each point. Processing software (SignalCalc, Data Physics, San Jose) was used to calculate FRFs from the excitation and response, and then to apply curve-fitting to extract

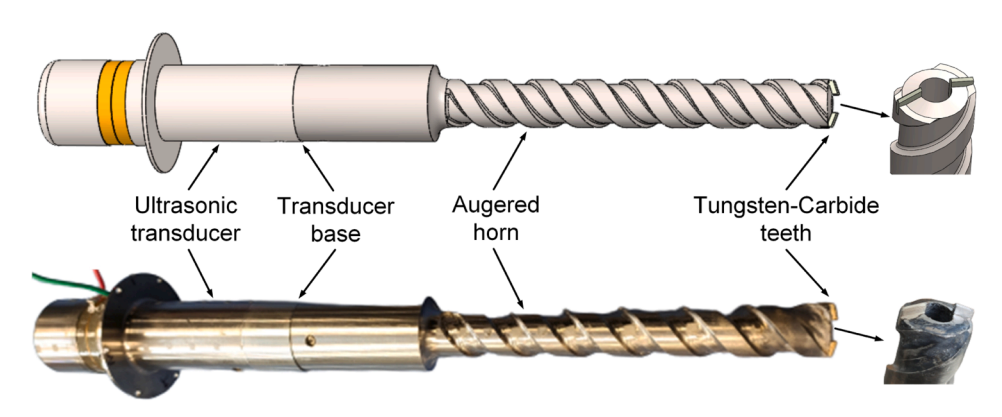
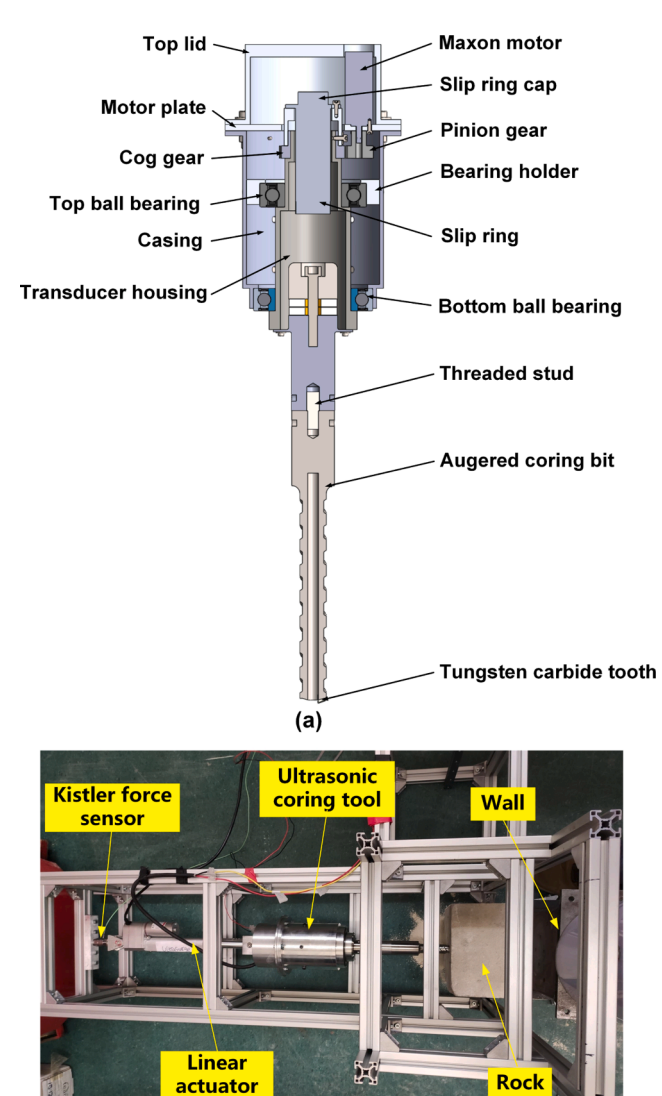


Fig. 2. The ultrasonic drill tool used in this study.



**Fig. 3.** Ultrasonic drilling experimental test rig: (a) ultrasonic drill tool assembly, (b) experimental test rig.

(b)

magnitude and phase. Finally, the FRFs were exported to modal analysis software (ME'scopeVES, Vibrant Technology, Denver) to extract modal parameters.

# 3.2. Experimental test rig

The ultrasonic drill system is presented in Fig. 3. The tool is fitted into a housing at its nodal flange, which is free to rotate and equipped with a spur gear. A pinion gear is fixed to a DC motor (476 rpm, 0.9 Nm maximal torque) to drive the spur. The gear ratio is 1:2.5, which provides 190 rpm at the tool, and a slip ring (MFS028-P0210-440V, MOFLON, Shenzhen) is used to supply power to the rotating ultrasonic assembly.

The ultrasonic assembly is driven forwards by a linear actuator (GLA750-P Gimson Robotics, Bristol), with its load path running through a force sensor/charge amplifier (9321B, 5015A, Kistler, Winterthur) to provide the weight-on-bit information. A benchtop power supply (BK9129B, BK Precision, Yorba Linda) is used to supply power to the motor and linear actuator. Power consumption on each channel can be recorded through an associated kit (IT-E132B) and LabView.

#### 3.3. Control system

Ultrasonically assisted machining (UAM) can often be carried out at constant feed rates, because the industrial substrate is usually a highly-repeatable material. However, in our experiment, the properties of the natural materials are inconsistent and a constant feed rate approach could lead to permanent contacts between the tool and the workpiece. This would disrupt the behaviour of the tool, and a different approach based on constant weight-on-bit (WOB) is therefore proposed instead.

The schematic for the WOB system is presented in Fig. 4 (a), and the control algorithm is shown in (b) [29]. In summary, this system uses a tunable bang-bang approach in constant pursuit of a target WOB, where that target may be varied as an experimental parameter.

This is executed using a square wave signal from an Arduino Uno board, with a high-level time duration  $T_1$  and a low-level time duration  $T_2$ . The measured weight-on-bit is averaged within  $T_1$ , then compared to the target value. The comparison will result in a decision to advance (if the cutting force is far below the target), not move (if the cutting force is within a dead zone centred on the target), or withdraw (if the cutting force is far above the target). This movement will then be carried out for the duration of  $T_2$ .

The dead zone is  $\pm \Delta\%$  of the target weight-on-bit, and the speed of the linear actuator cannot exceed 3 mm/s. After iteration,  $T_1=10$  ms,  $T_2=300$  ms and  $\Delta=10$  have been chosen to execute the control loop. These parameters, which essentially give up to approximately three 1 mm control movements per second, were then held constant throughout the study.

This autonomous control loop therefore ensures that near-constant WOB is maintained, regardless of the inconsistencies of the rock being drilled, ensuring that some tool separation is maintained. This, in turn, ensures that the phase-tracking mode stabilisation technique will work effectively.

#### 4. Results and discussion

# 4.1. Characterisation of the ultrasonic drill tool

The electromechanical coupling coefficient of the drill tool, 0.12, can be calculated from the resonance and anti-resonance frequencies in Fig. 5. The mechanical Q factor, 620, can also be calculated from the impedance measurement. The phase angle at the resonance frequency is equal to  $24.5 \ degrees$ .

Fig. 6 shows the predicted and measured operating modes. During simulation, a full integrated electromechanical model is created in finite element analysis software (Abaqus-Simulia, Dassault Systèmes, Vélizy-Villacoublay, France), and the dimensionless longitudinal amplitude is acquired from the eigenfrequency-eigenmode identification.

Both waveforms suggest that there are three nodes in the ultrasonic drill tool, located at the transducer flange, at the step, and roughly one-third of the way along the auger section. This confirms that the ultrasonic drill tool will operate at its third longitudinal mode (L3) at around 20 kHz. The gain, defined as the ratio between the amplitude at the teeth of and the amplitude at the back mass, shows an agreement of approximately five.

Due to the auger features, some torsional output is generated alongside the longitudinal mode. To quantify the torsionality (defined as the torsional amplitude in proportion to the longitudinal amplitude), the tangential direction (Y) amplitude and longitudinal direction (Z) amplitude at different transducer base excitation levels were measured at the lateral surface of the cutting tooth, as shown in Fig. 7. Similarly, the dimensionless tangential amplitude and longitudinal amplitude were acquired from the finite element analysis. Both measurements were taken at the same point on the tooth.

The simulated torsionality of the drill tool is slightly under 8%. As the excitation of the transducer was increased in experiment, the measured torsionality varied between 10% and 8%, showing a generally

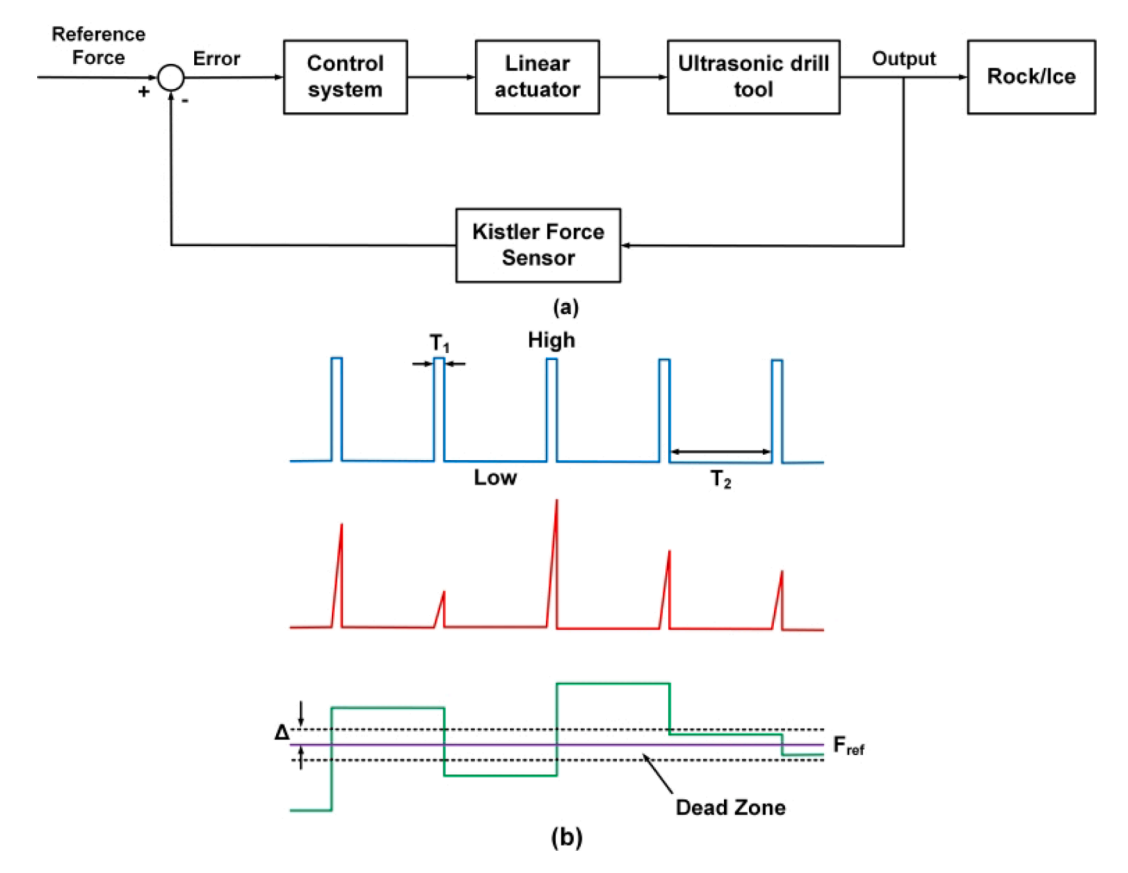


Fig. 4. Ultrasonic drill tool control design: (a) schematic control diagram, (b) control algorithm.

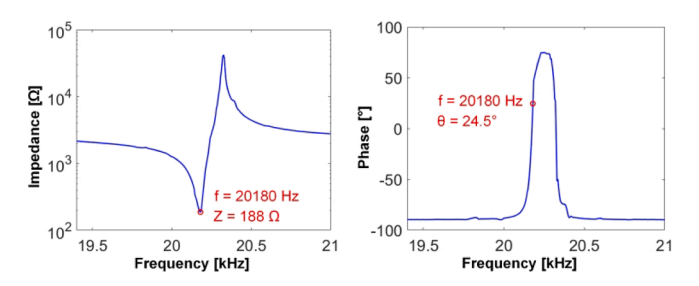
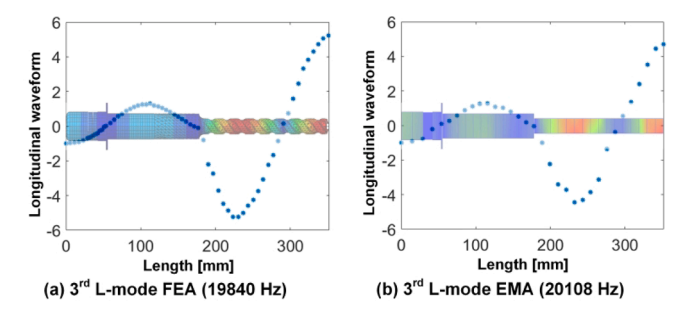


Fig. 5. Impedance and phase characteristics of the drill tool.



 $\begin{tabular}{ll} Fig. 6. Predicted and measured longitudinal waveform of the ultrasonic drill tool. \end{tabular}$ 

good agreement in performance.

# 4.2. Drilling experiments in the rocks

During rock drilling experiments, applied weight-on-bit and the

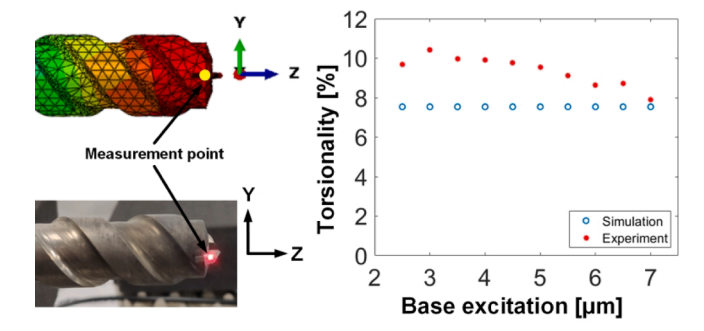


Fig. 7. Torsionality identification of the ultrasonic drill tool.

displacement amplitude at the cutting teeth were varied. A new set of cutting teeth was fitted for each new analogue material, before each drill cycle, to minimise the effect of tool wear on the drilling performance.

Vibration amplitudes of 0  $\mu m,~2.5~\mu m,~5.0~\mu m,~7.5~\mu m,~and~10~\mu m$  peak-to-peak were selected, then generated by the P100 control unit at the base of the transducer (Fig. 2). These correspond to 0  $\mu m,~9.2~\mu m,~18.2~\mu m,~27.4~\mu m,~and~36.6~\mu m$  at the cutting teeth. This gain was confirmed by 1-D laser Doppler vibrometer measurements.

N, 100 N and 150 N were chosen as target weights-on-bit, allowing the control loop to be set as per Fig. 4.

# 4.2.1. Rate of progress

The penetration results for aircrete, limestone, marble, and tuff are shown in Fig. 8. These experiments lead to boreholes such as those shown in Fig. 9, and are summarised in Fig. 10.

In aircrete and limestone, maximum depth was attained for all combinations of amplitude and WOB. The curves are highly linear, and show that ultrasonic vibration consistently accelerates progress.

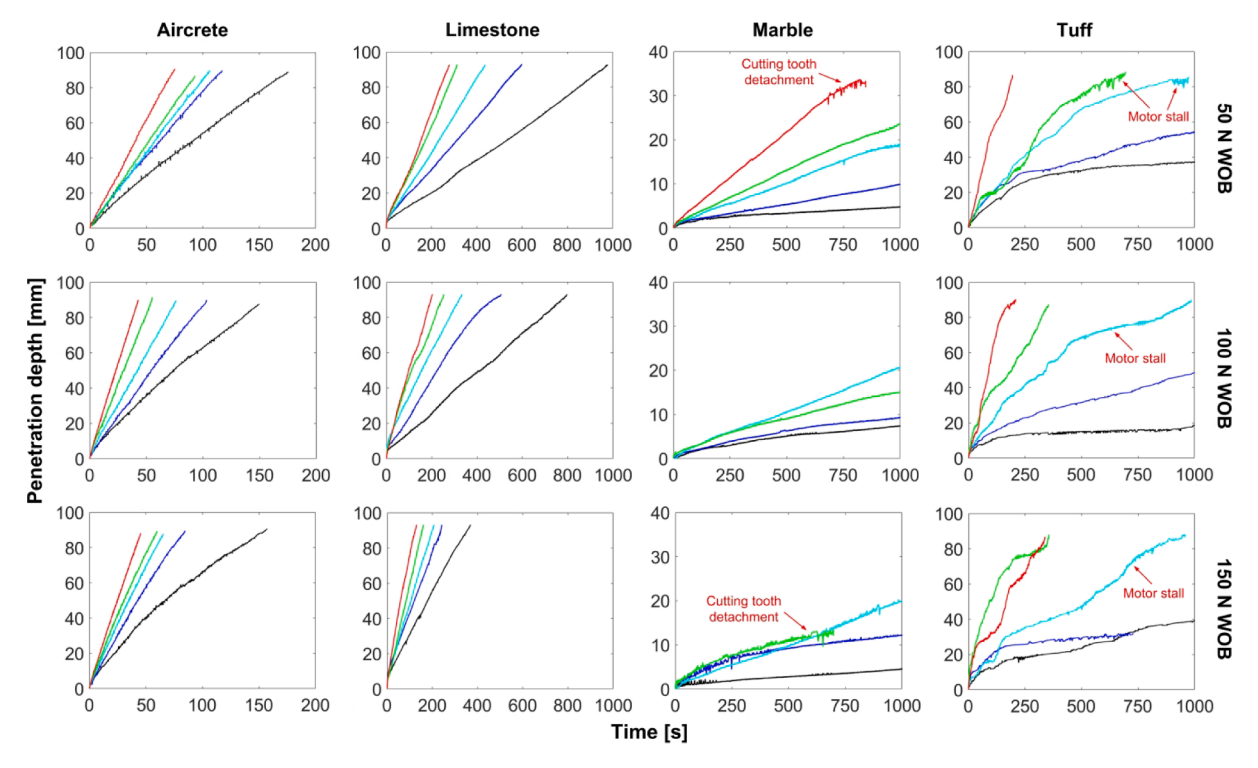


Fig. 8. Penetration depths against time and target weight-on-bit (WOB) in aircrete, limestone, marble and tuff: black 0  $\mu$ m, blue 9.2  $\mu$ m, cyan 18.2  $\mu$ m, green 27.4  $\mu$ m, and red 36.6  $\mu$ m of vibration amplitude at the cutting teeth.



Fig. 9. UAD drill holes in aircrete, limestone, marble and tuff.

In marble, higher amplitude and WOB led to detachment of the teeth in the most aggressive scenarios, but the broad trends of enhanced progress with increasing amplitude, as seen in aircrete and limestone, were otherwise repeated. Where teeth became separated, they remained trapped under the tool and left burn marks in the material.

Finally, in tuff, although the broad trends were still present, the performance was less repeatable due to the heterogeneous nature of the material. Motor stalls (which were sometimes irreversible) were also common, and may have been associated with damp regions in the porous material.

Fig. 11 shows the average power consumption of the ultrasonic system, rotation system, linear actuator, added together to give total power throughout each drill cycle.

In aircrete and limestone, investing in ultrasonic power consistently reduced torque motor power, but not enough to prevent an increased power requirement overall.

In marble and tuff these savings in torque motor power did not appear, but these result sets are somewhat questionable due to the tooth detachment and jamming events baked into the data.

# 4.2.2. Power and energy consumption

The specific energy consumption, calculated from the power levels in

Fig. 11 (multiplied by the relevant cycle duration), is shown in Fig. 12.

There are clearly energy optima in aircrete and limestone, a possible energy optimum in marble, but no energy optimum in the unpredictable tuff.

#### 4.2.3. Ultrasonically assisted drilling vs conventional drilling

To further demonstrate the effect, the transducer was cycled on and off during dedicated experimental runs (100 N weight-on-bit, 18.2  $\mu m$  amplitude). The results are shown in Fig. 13.

In each case, the run began with the ultrasonics off and there was an initial period of rapid progress as the teeth become fully engaged. Once this period was past the ultrasonics were cycled.

In aircrete and limestone, ultrasonic vibration immediately and significantly increased rate-of-progress. In marble, the effect was less pronounced, but still visible. In tuff, there was not an immediate acceleration but, when the ultrasonic vibration was turned off, the rate-of-progress collapsed.

#### 4.3. Drilling experiments in the ice

The drilling experiments in ice were difficult, and only a few runs were undertaken due to constant tooth detachments. One of these runs is

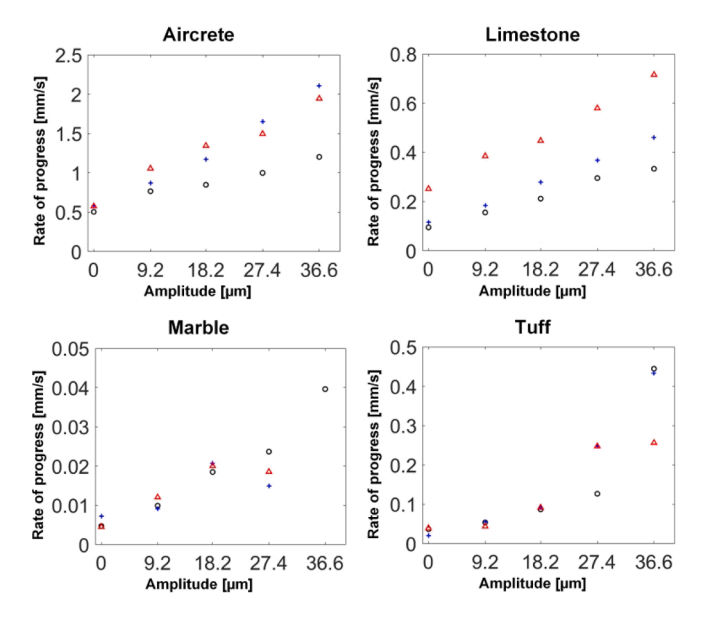


Fig. 10. Rate of progress variation with amplitude and weight-on-bit: O 50 N WOB, + 100 N WOB,  $\Delta$  150 N WOB.

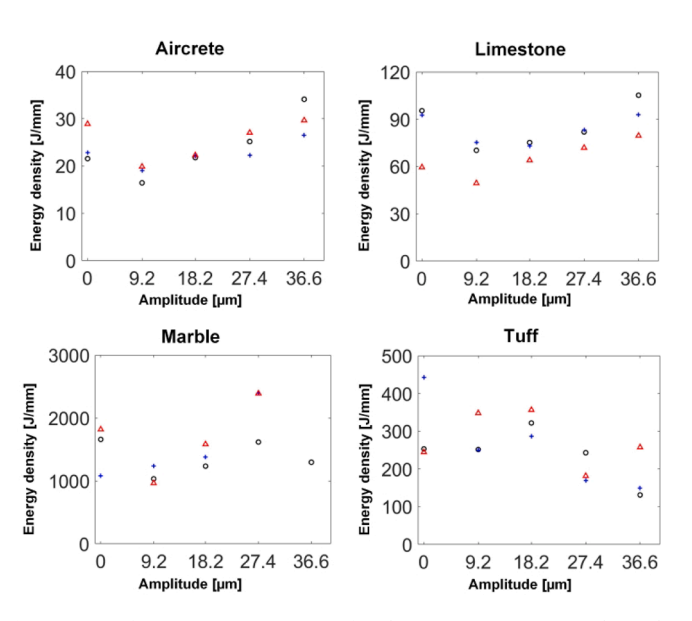


Fig. 12. Specific energy use, in terms of joules per mm progress, with amplitude and weight-on-bit: O 50 N, + 100 N,  $\Delta$  150 N target weight-on-bit (WOB).

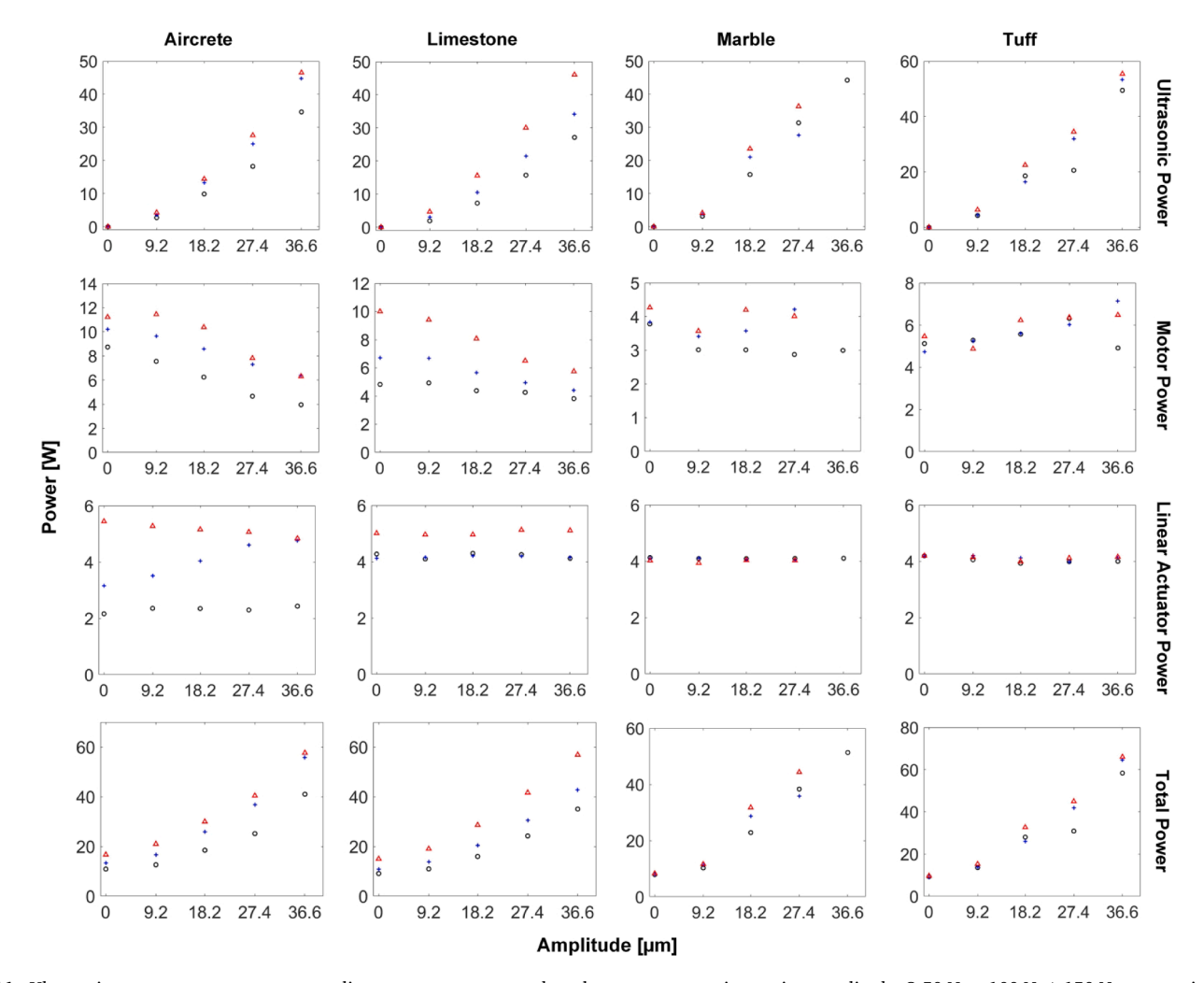


Fig. 11. Ultrasonic power, torque motor power, linear actuator power and total power consumption against amplitude: O 50 N, + 100 N,  $\Delta$  150 N target weight-on-bit (WOB).

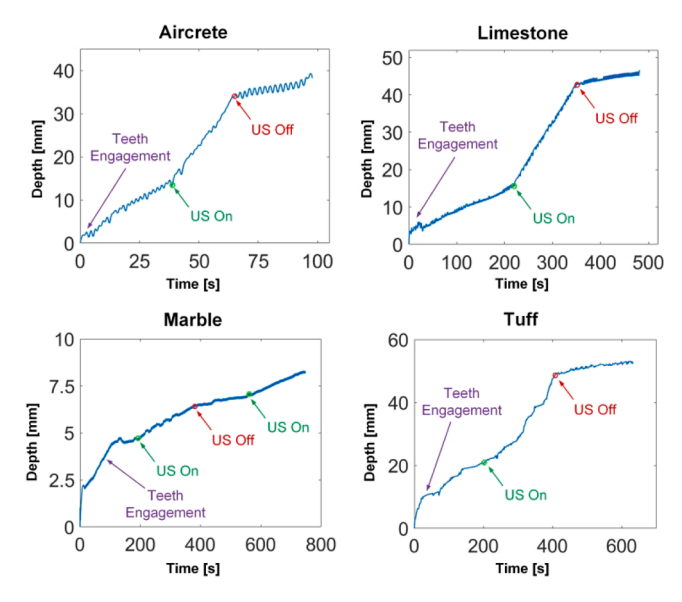


Fig. 13. Comparison of UAD and conventional drilling of aircrete, limestone, marble and tuff.

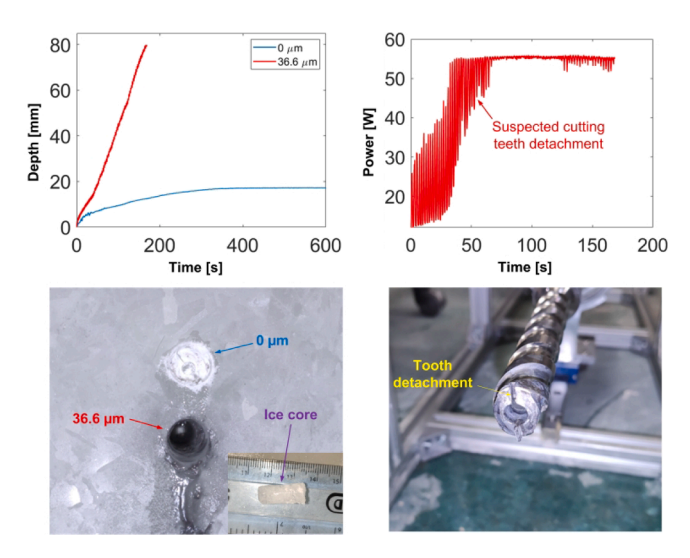


Fig. 14. UAD (36.6  $\mu m$ ) and conventional drilling in ice.

presented in Fig. 14, which shows a conventional run experiencing saturation and a UAD run with excellent progress. Both runs were conducted at 50 N WOB.

However, the power consumption in the UAD run behaved oddly, and it is suspected that one tooth was lost at 50 s while the drill cycle continued on the other tooth alone. Only the surviving tooth was found to be attached when the tool was removed from the hole afterwards.

We believe that meltwater around the teeth began to cavitate, and this cavitation eroded the silver solder bond [30]. To validate this effect, the ultrasonic drill tool with two newly soldered teeth was inserted into a cup of water, and both teeth fell off in less than one minute.

# 5. Conclusion

This paper presents the experimental results arising from the application of a UAD tool to different types of rocks and ice, at a range of ultrasonic amplitudes, with an autonomous system maintaining a series of prescribed weight-on-bit values.

In relatively soft aircrete and limestone, near-linear results show rate of progress increasing with both weight-on-bit (50 N to 150 N) and

ultrasonic amplitude (0  $\mu$ m to 36.6  $\mu$ m). In our experiments, an amplitude of 9.2  $\mu$ m resulted in the lowest energy consumption per unit depth.

The harder marble was more challenging, but again there is some evidence that  $9.2~\mu m$  represented an energy optimum.

The results in tuff are harder to interpret, given the non-homogenous nature of the material. Nonetheless, there is little doubt that the application of ultrasonic vibration had a generally positive effect on rate of progress.

Finally, in ice, there are very positive indications, but the teeth were consistently unable to survive the drilling process.

# **Declaration of Competing Interest**

The authors declare that they have no known competing financial interests or personal relationships that could have appeared to influence the work reported in this paper.

#### Data availability

Data will be made available on request.

#### Acknowledgement

The authors thank the University of Glasgow for allowing the research to be carried out in the Hammermen Laboratory in James Watt School of Engineering.

#### References

- [1] R. Timoney, K. Worrall, D. Firstbrook, P. Harkness, J. Rix, D. Ashurst, R. Mulvaney, M.J. Bentley, A low resource subglacial bedrock sampler: The percussive rapid access isotope drill (P-RAID), Cold Reg. Sci. Technol. 177 (2020), 103113.
- [2] G. Briggs, A. Gross, Technical Challenges of Drilling on Mars. 40<sup>th</sup> AIAA Aerospace Sciences Meeting & Exhibit, 2002.
- [3] K. Zacny, G. Paulsen, M. Szczesiak, Challenges and Methods of Drilling on the Moon and Mars, IEEE Aerospace Conference (2011).
- [4] B.J. Glass, S. Thompson, G. Paulsen, "Robotic Planetary Drill Tests," The International Symposium on Artificial Intelligence, Robotics, and Automation in Space (i-SAIRAS), 2010.
- [5] Y. Bar-cohen, S. Sherrit, B.P. Dolgin, X. Bao, Z. Chang, D.S. Pal, R. Krahe, J. Kroh, S. Du, T. Peterson, "Ultrasonic/sonic drilling/coring (USDC) for planetary applications," Proceedings of SPIE's 8<sup>th</sup> Annual International Symposium on Smart Structures and Materials, no. 4327-55, pp. 1-7, 2001.
- [6] S. Sherrit, B.P. Dolgin, Y. Bar-cohen, D.S. Pal, J. Kroh, T. Peterson, Modeling of Horns for Sonic/Ultrasonic Applications, IEEE Ultrasonics Sumposium (1999).
- [7] P. Harkness, M. Lucas, A. Cardoni, Maximization of the Effective Impulse Delivered by a High-Frequency/Low-Frequency Planetary Drill Tool, IEEE Trans. Ultrasonics, Ferroelectrics, and Frequency Control 58 (11) (2011) 2387–2396.
- [8] X. Li, M. Lucas, P. Harkness, Full and Half-Wavelength Ultrasonic Percussive Drills, IEEE Trans. Ultrason. Ferroelectr. Freq. Control 65 (11) (2018) 2150–2159.
- [9] V.K. Astashev, V.I. Babitsky, Ultrasonic Processes and Machines, Springer-Verlag, Berlin Heidelberg, 2007.
- [10] V.V. Silberschmidt, S.M.A. Mahdy, M.A. Gouda, A. Naseer, A. Maurotto, A. Roy, Surface-roughness improvement in ultrasonically assisted turning, Procedia CIRP 13 (2014) 49–54.
- [11] W.-X. Xu, L.-C. Zhang, Ultrasonic vibration-assisted machining: principle, design and application, Adv. Manuf. 3 (3) (2015) 173–192.
- [12] V.K. Astashev, V.I. Babitsky, Ultrasonic cutting as a nonlinear (vibro-impact) process, Ultrasonics 36 (1-5) (1998) 89–96.
- [13] V.I. Babitsky, V.K. Astashev, A.N. Kalashnikov, Autoresonant control of nonlinear mode in ultrasonic transducer for machining applications, Ultrasonics 42 (1-9) (2004) 29–35.
- [14] J. Dassow, X. Li, M.R. Lee, M. Young, P. Harkness, Ultrasonic drilling for the characterisation of building stones and salt induced decay, Ultrasonics 101 (2020) 106018, https://doi.org/10.1016/j.ultras.2019.106018.
- [15] X. Peng, L. Li, Y. Yang, G. Zhao, T. Zeng, Experimental study on rotary ultrasonic vibration assisted drilling rock, Adv. Space Res. 67 (1) (2021) 546–556.
- [16] N.V. Mikhailova, P.Y. Onawumi, A. Roy, V.V. Silberschmidt, Ultrasonically Assisted Drilling of Rocks, AIP Conf. Proc. 1959 (1) (2018) 1–5.
- [17] A. Ahmed, J. Kamau, Advantages and Implications of Low Density Aircrete Products for the Construction Industry, Int. J. Sci., Environ. Technol. 6 (3) (2017) 1758–1767.
- [18] http://www.geol-amu.org/notes/m10-1-1b.htm.
- [19] G.E. Manger, Porosity and Bulk Density of Sedimentary Rocks: Contributions to Geochemistry, Geological Survey Bulletin, Vol. 1144-E, 1963.

- [20] E. Korneeva, M.S.S. Mohanad, A. Babanina, E. Zaytsev, S. Poberezhskii, Operational characteristics of limestone and methods to increase its strength, E3S Web of Conferences 91 (02028) (2019) 1–8.
- [21] G.M.A. Wahab, M. Gouda, G. Ibrahim, Study of physical and mechanical properties for some of Eastern Desert dimension marble and granite utilized in building decoration, Ain Shams Eng. J. 10 (4) (2019) 907–915.
- [22] P. Dobson, S. Nakagawa, Summary of Rock-Property Measurements for Hong Kong Tuff Samples, Ernest Orlando Lawrence Berkeley National Laboratory, no. LBNL-58878, 2005, pp. 1-9.
- [23] A.A. Barahim, I.A. Al-Akhaly, I.R. Shamsan, Engineering Properties of Volcanic Tuff from the Western Part of Yemen, SQU Journal for Science 22 (2) (2017) 81–88
- [24] https://messenger.jhuapl.edu/Learn/pdf/ice\_mineral.pdf.
- [25] K. F. Voitkovskii, "The Mechanical Properties of Ice.".
- [26] G. Paulsen, Z. Mank, A. Wang, P. Chow, C. Hyman, T. Thomas, A. Lee, K. Zacny, J. Smith, J. Quinn, E. Mumm, R. Hayes, The Regolith and Ice Drill for Exploration

- of New Terrains (TRIDENT); a One-Meter Drill for the Lunar Resource Prospector Mission, in: Proceedings of the  $44^{th}$  Aerospace Mechanisms Symposium, 2018, pp. 13–25.
- [27] A. Caronti, R. Carotenuto, M. Pappalardo, Electromechanical coupling factor of capacitive micromachined ultrasonic transducers, J. Acoust. Soc. America 113 (1) (2003) 279–288.
- [28] P. Avitabile, Experimental Modal Analysis, Sound and Vibration Magazine 35 (1) (2001) 1–15.
- [29] X. Li, K. Worrall, P. Harkness, R. Timoney, A. Bolhovitins, M. Lucas, A motion control system design for an Ultrasonic Percussive Coring/Drilling (UPCD) unit, in: AIAA Space 2015 Conference and Exposition, 2015, pp. 1–13.
- [30] Z. Li, Z. Xu, L. Ma, S. Wang, X. Liu, J. Yan, Cavitation at filler metal/substrate interface during ultrasonic-assisted soldering. Part II: Cavitation erosion effect, Ultrasonics - Sonochemistry 50 (2019) 278–288.